

MAJOR PAPER

Differentiating Liver Hemangioma from Metastatic Tumor Using T2-enhanced Spin-echo Imaging with a Time-reversed Gradient-echo Sequence in the Hepatobiliary Phase of Gadoteric Acid-enhanced MR Imaging

Yukihisa Takayama¹, Akihiro Nishie^{1*}, Daisuke Okamoto¹, Nobuhiro Fujita¹,
Yoshiki Asayama², Yasuhiro Ushijima¹, Tomoharu Yoshizumi³, Masami Yoneyama⁴,
and Kousei Ishigami¹

Purpose: To evaluate the utility of T2-enhanced spin-echo imaging using the time-reversed gradient echo sequence (T2FFE imaging) in the hepatobiliary phase (HBP) of gadoteric acid-enhanced MRI (Gd-EOB-MRI) for differentiating hemangiomas from metastatic tumors.

Methods: A total of 61 patients with 133 liver lesions, including 37 hemangiomas and 96 metastatic tumors, were scanned by Gd-EOB-MRI. Four data sets were independently analyzed by two readers: (1) 3D fat-suppressed T2-weighted imaging (FS-T2WI) alone; (2) the combination of 3D FS-T2WI and T2FFE imaging in the HBP of Gd-EOB-MRI; (3) the combination of 3D FS-T2WI, diffusion-weighted imaging (DWI) with the b-value of 1000 s/mm² and the apparent diffusion coefficient (ADC); and (4) a dynamic study of Gd-EOB-MRI. After classifying the lesion sizes as ≤ 10 mm or > 10 mm, we conducted a receiver-operating characteristic analysis to compare diagnostic accuracies among the four data sets for differentiating hemangiomas from metastatic tumors.

Results: The areas under the curves (AUCs) of the four data sets of two readers were: (1) ≤ 10 mm (0.85 and 0.91) and > 10 mm (0.88 and 0.97), (2) ≤ 10 mm (0.94 and 0.94) and > 10 mm (0.96 and 0.95), (3) ≤ 10 mm (0.90 and 0.87) and > 10 mm (0.89 and 0.95), and (4) ≤ 10 mm (0.62 and 0.67) and > 10 mm (0.76 and 0.71), respectively. Data sets (2) and (3) showed no significant differences in AUCs, but both showed significantly higher AUCs compared to that of (4) regardless of the lesion size ($P < 0.05$).

Conclusion: The combination of 3D FS-T2WI and T2FFE imaging in the HBP of Gd-EOB-MRI achieved an accuracy equivalent to that of the combination of 3D FS-T2WI, DWI, and ADC and might be helpful in differentiating hemangiomas from metastatic tumors.

Keywords: gadoteric acid-enhanced magnetic resonance imaging, liver hemangioma, metastatic tumor, T2-enhanced time-reversed gradient echo sequence

¹Department of Clinical Radiology, Graduate School of Medical Sciences, Kyushu University, Fukuoka, Fukuoka, Japan

²Department of Advanced Imaging and Interventional Radiology, Graduate School of Medical Sciences, Kyushu University, Fukuoka, Fukuoka, Japan

³Department of Surgery and Science, Graduate School of Medical Sciences, Kyushu University, Fukuoka, Fukuoka, Japan

⁴Philips Electronics Japan, Tokyo, Japan

*Corresponding author: Department of Clinical Radiology, Graduate School of Medical Sciences, Kyushu University, 3-1-1, Maidashi, Higashi-ku, Fukuoka, Fukuoka 812-8582, Japan. Phone: +81-92-642-5695, Fax: +81-92-642-5708, E-mail: anishie@radiol.med.kyushu-u.ac.jp



This work is licensed under a Creative Commons Attribution-NonCommercial-NoDerivatives International License.

©2021 Japanese Society for Magnetic Resonance in Medicine

Received: October 7, 2020 | Accepted: March 19, 2021

Introduction

Gadoteric acid-enhanced MRI (Gd-EOB-MRI) is widely used for the assessment of benign and malignant liver lesions, such as hemangioma, hyperplasia, adenoma, hepatocellular carcinoma, cholangiocellular carcinoma, and metastatic tumors.^{1–6} Several research groups have investigated the strategies for differentiating hemangiomas from metastatic tumors on liver MRI.^{7–13} Reliable findings for the differentiation include the enhancement pattern in the arterial phase, plus the lesion's signal intensity (SI) on T2-weighted imaging (T2WI) and diffusion-weighted imaging (DWI).^{7,9,11,14} Hepatobiliary phase (HBP) images of Gd-EOB-MRI are not useful for the differentiation of

hemangiomas from metastatic tumors because both lesions show hypointensity. However, image degradation in the arterial phase of Gd-EOB-MRI disturbs the image interpretation and diagnosis at the frequency of 13%–25%.¹⁵ In these cases, it can be difficult to differentiate hemangiomas from metastatic tumors. If another MR sequence could be used to differentiate between hemangiomas and metastatic tumors, it would contribute to the diagnostic performance of Gd-EOB-MRI.

A T2-enhanced spin echo using a time-reversed gradient echo sequence (T2-fast field echo: T2FFE) is a sequence in which the signal acquired is a spin echo (or Hahn echo).^{16,17} The SI values of organs or lesions are characterized by T2 relaxation, with a TE equal to $2 \times TR - TE$, where the TR and TE are of the original gradient echo (GRE) sequence before time reversal.¹⁶ Interestingly, the T2FFE sequence also has a high sensitivity to T1 shortening effects due to gadoteric acid, depending on the flip angle (FA).¹⁸ After optimization of the FA, T2FFE imaging in the HBP of Gd-EOB-MRI is useful for differentiating benign versus malignant liver lesions by means of the interpretation of the lesions' SI values.¹⁸ We thus hypothesized that the T2FFE imaging to Gd-EOB-MRI might contribute to the differentiation of hemangiomas from metastatic tumors. The purpose of this study was to evaluate the utility of lesion's SI on T2FFE imaging in the HBP of Gd-EOB-MRI for differentiating hemangioma from metastatic tumor.

Materials and Methods

Subjects

The study was approved by our institutional review board, and the requirement of written informed consent was waived because this study was a retrospective analysis. We first investigated the records of 602 patients who had undergone Gd-EOB-MRI at our institute during the period from December 2013 to December 2014. Patients were selected referring to the following criteria. The inclusion criteria were as follows: (1) the patient had undergone Gd-EOB-MRI on a 1.5T MR system; and (2) the patient had or was suspected of having a hemangioma or a metastatic tumor. The exclusion criteria were as follows: (1) an MR contrast agent other than gadoteric acid was used; (2) an MR contrast agent was not used because of a contraindication for contrast media; (3) the patient had or was suspected of having another type of liver lesion such as hepatocellular carcinoma or cholangiocellular carcinoma; and (4) it was difficult to diagnose a liver lesion on imaging including those in a follow-up study, or there was no pathology result. A summary flowchart of the patient selection is presented in Fig. 1. After applying these criteria, a total of 61 patients were enrolled in this study. We categorized the liver function of all enrolled patients as Child-Pugh type A based on the patients' clinical data. The other characteristics of the 61 patients are summarized in Table 1.

All liver lesions in the 61 patients were retrospectively reviewed by this study's coordinator (Y.T., with 20 years of experience in liver MRI interpretation). Five hemangiomas in one patient and 50 metastatic tumors in 21 patients were surgically resected, and the histopathological results were used for the diagnosis of the lesion. For the other 32 hemangiomas in 18 patients and 46 metastatic tumors in 21 patients, typical imaging findings of dynamic contrast-enhanced computed tomography (DCE-CT) and the interval change in the lesion size during the patient's follow-up were used for the diagnosis after the study coordinators reviewed the patient's imaging findings and medical records.

Hemangiomas were diagnosed based on the findings revealed by DCE-CT, including dot-like enhancement with a subsequent contrast filling pattern, flash-filling enhancement pattern, or very delayed fill-in pattern, and the absence of lesion size change in follow-up imaging studies at > 6 months.^{9,19–22} Metastatic tumors were diagnosed based on the patient's history of malignancy, DCE-CT findings (including ring enhancement), elevated tumor markers (e.g., carcinoembryonic antigen for colon and rectal cancers, and carbohydrate antigen 19-9 for pancreas cancer), and follow-up imaging studies at > 6 months, which showed tumor shrinkage with treatment or tumor progression without treatment.^{9,23,24} After these criteria were applied, a total of 133 liver lesions were analyzed in this study (Table 1).

MRI

All MR examinations were performed using a 1.5T whole-body clinical system (Achieva, Philips Healthcare, Best, the Netherlands) with sensitivity-encoding acceleration (SENSE) techniques using a 32-channel phased-array coil. The MR examinations were limited to 1.5T because of the specific absorption ratio (SAR) limitation in the FA setting of the T2FFE sequence.¹⁸ For dynamic studies including arterial (first), second, transitional, and HB phases, 3D fat-suppressed GRE T1-weighted imaging (T1WI) was performed. A total amount of gadoteric acid (EOB Primovist; Bayer Yakuin, Osaka, Japan) based on the patient's body weight (0.1 mL/kg) was intravenously injected. The scan timing of the arterial phase of the dynamic study was determined by a test injection method.²⁵ The second phase was 30 sec after the arterial phase, and the transitional phase was 180 sec after injection of contrast agent.

The 3D fat-suppressed T2-weighted imaging (FS-T2WI) was performed using spectral presaturation with inversion recovery (SPIR) and volume isotropic turbo spin-echo acquisition (VISTA) with low constant variable FA techniques.²⁴ For the HBP, images were obtained at ≥ 20 min after the start of the injection of the contrast agent. The 3D FS-T2WI, T2FFE imaging, DWI, and 3D T1WI were scanned in sequence. In addition to the MR imaging, an apparent diffusion coefficient (ADC) map was developed using a mono-exponential model that was estimated from the slope of the linear regression line fitted to the natural

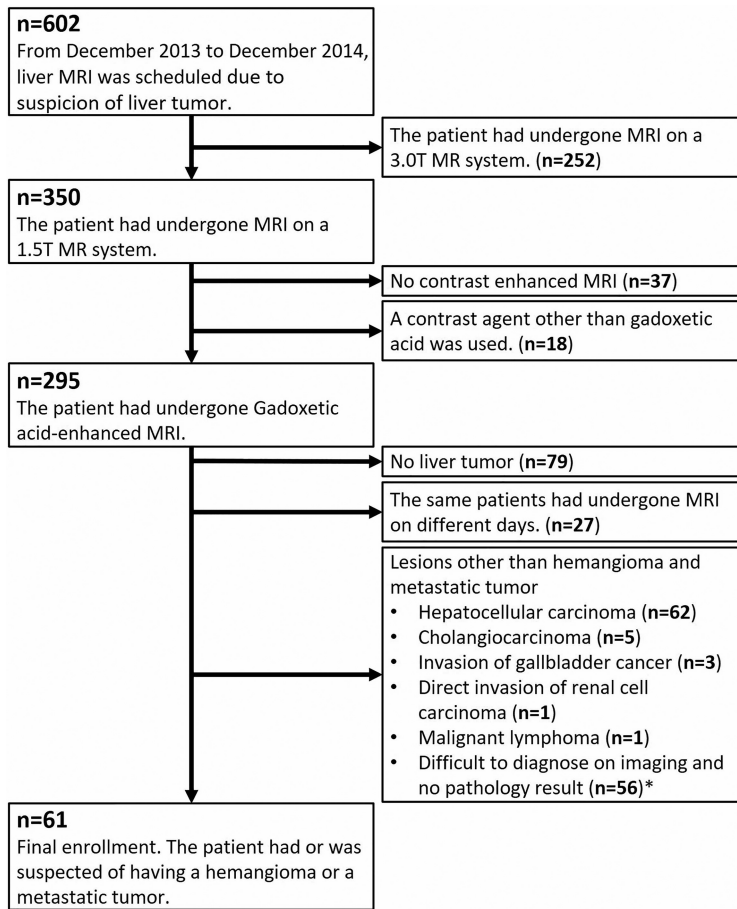


Fig. 1 A summary flowchart of the patient selection. *: The initial diagnosis and actual outcome of liver lesions in the 56 patients who were excluded by criteria are shown in Appendix 1.

logarithm of signal intensities of DWI with b-values of 0, 500, and 1000 s/mm². Details of the MR parameters are shown in Table 2.

The lesion-to-nonlesion contrast ratios of 3D T1WI, 3D FS-T2WI, and T2FFE imaging

The lesion-to-nonlesion contrast ratios (CRs) of the hemangiomas and metastatic tumors on 3D T1WI, 3D FS-T2WI, and T2FFE imaging in the HBP of the Gd-EOB-MRI were independently calculated by two radiologists (the study coordinator Y.T. and another experienced abdominal radiologist, A.N., with 26 years of experience in liver MRI interpretation).

The lesion-to-nonlesion CR was calculated using the following formula:

$$(SI_{\text{lesion}} - SI_{\text{liver}}) / SI_{\text{liver}},$$

where SI_{lesion} is the signal intensity of the hemangioma or metastatic tumor, and SI_{liver} is the signal intensity of the liver parenchyma.

First, the ROIs of each liver lesion and the liver parenchyma were drawn on 3D T1WI. Image slices in which the liver lesion showed the maximum diameter on transverse

images were selected. For each liver lesion, an ROI that was as large as possible was drawn on the lesion.

For the ROIs of the liver parenchyma, three ROIs (as large as possible) were drawn with care taken to avoid the intrahepatic bile duct and vessels. SI_{liver} was defined as the average value of the three SIs measured. Next, the ROIs on the 3D T1WI were copied on the 3D FS-T2WI and the T2FFE. All ROI measurements were performed using a commercially available picture archiving and communication system (SYNAPSE, FujiFilm, Tokyo). Measurements of the lesion-to-nonlesion CR were repeated three times for each lesion, and the averaged values were used for the analysis.

The comparison of diagnostic accuracy among the four data sets

Four different imaging data sets were prepared for the analysis: (1) 3D FS-T2WI alone; (2) the combination of 3D FS-T2WI and T2FFE imaging in the HBP of Gd-EOB-MRI; (3) the combination of 3D FS-T2WI and DWI with the b-value of 1000 s/mm² and an ADC map; and (4) dynamic Gd-EOB-MRI including the pre-contrast, arterial, second, transitional, and HBPs. We did not analyze 3D T1WI in the HBP of

Table 1 Characteristics of the 61 patients and 133 liver lesions analyzed

Characteristics	n
Males/females	36/25
Age range (mean)	32–83 (62.0) years
Child-Pugh Classification A/B/C	61/0/0
Patients with hemangioma	19
Patients with metastatic tumor	42
Primary site of metastatic tumors:	
<i>Rectal cancer</i>	14
<i>Colon cancer</i>	15
<i>Pancreas cancer</i>	5
<i>Gastrointestinal stromal tumor</i>	3
<i>Pancreatic neuroendocrine tumor</i>	2
<i>Bile duct cancer</i>	1
<i>Lung cancer</i>	1
<i>Epipharyngeal cancer</i>	1
Analyzed liver lesions (n = 133)	n
Hemangioma	37
Size range (mean):	7–70 (19.6) mm
≤ 10 mm	11
> 10 mm	26
Diagnosis:	
Histopathology	5
Imaging findings	32
Metastatic tumor	96
Size range (mean):	7–70 (18.7) mm
≤ 10 mm	27
> 10 mm	69
Diagnosis:	
Histopathology	50
Imaging and clinical findings	46

Gd-EOB-MRI for data sets (1), (2), and (3), but HBP images were used for the localization of liver lesions.

The images were independently interpreted by two experienced abdominal radiologists (D.O. and N.F. with 18 and 17 years of experience in interpreting liver MRI, respectively). They were blinded to all clinical information, including the MRI reports, the patients' clinical data, and all imaging data reviewed by the study coordinator. The study coordinator presented each imaging set in random order in terms of patients to each reader separately with information about the liver segment and the number of liver lesions. For patients

with multiple liver lesions, a maximum of the five largest liver lesions per single patient was selected by the coordinator beforehand and those liver lesions were used for the analysis. Image interpretation was performed three times at 4-week intervals in the order of imaging sets (1), (2), (3), and (4).

The two readers interpreted each combination of imaging set and diagnosed liver lesion(s) as a hemangioma or metastatic tumor by using a 4-point scale: 1 point for a liver hemangioma, 2 points for a possible liver hemangioma, 3 points for a possible metastatic tumor, and 4 points for a metastatic tumor. We considered liver lesions with 1 or 2 points as liver hemangiomas and those with 3 or 4 points as metastatic tumors.

The diagnostic criteria of hemangioma on imaging were as follows: On the 3D FS-T2WI, the lesion's SI was high (similar to water's SI), and for the T2FFE imaging, the lesion showed an apparently high SI compared to liver parenchyma, and the high-SI area of the lesion was $\geq 50\%$.^{9,26} Otherwise, a lesion was diagnosed as a metastatic tumor. On the DWI, the lesion's SI was high on DWI with the b-value of 1000 s/mm^2 , and the ADC of the liver lesion was higher than that of the liver parenchyma.^{27,28} If a lesion's SI was high on DWI with the b-value of 1000 s/mm^2 and the ADC of a liver lesion was equal to or lower than that of the liver parenchyma, the lesion was diagnosed as a metastatic tumor. If there was a divergence in judgement between the two sequences during the interpretation of the combination of 3D FS-T2WI and T2FFE imaging or of the combination of 3D FS-T2WI and DWI with the b-value of 1000 s/mm^2 and an ADC map, the findings obtained with the T2FFE imaging and the DWI/ADC map were prioritized.

For the dynamic Gd-EOB-MRI, the diagnostic criteria of hemangioma were dot-like enhancement with a subsequent contrast filling pattern, flash-filling enhancement pattern, or very delayed fill-in pattern.^{9,19–22} Metastatic tumors were diagnosed based on the appearance of ring enhancement on the arterial phase of DCE-MRI without a subsequent contrast filling pattern or target appearance in the HBP.²⁹

Statistical analyses

The lesion-to-nonlesion CRs between the hemangiomas and metastatic tumors on 3D T1WI, 3D FS-T2WI, and T2FFE imaging were compared by Student's t-test. We calculated the intraclass correlation coefficient (ICC) using a two-way random-effects model to describe the correlations of the measurements of 3D T1WI, 3D FS-T2WI, and T2FFE imaging between the two readers based on the following criteria: < 0.40 , poor agreement; $0.40–0.59$, fair agreement; $0.60–0.74$, good agreement; and ≥ 0.75 , excellent agreement.

For the determination of the diagnostic accuracy for differentiating hemangiomas from metastatic tumors, we performed a receiver operating characteristic (ROC) analysis to calculate the area under the curve (AUC). AUCs were separately calculated after liver lesions were categorized into two groups:

Table 2 Details of the sequence parameters

Unit		3D T1WI	3D FS-T2WI	T2FFE imaging	DWI
Imaging technique		eTHRIVE	VISTA	T2-enhanced spin echo using time-reversed gradient echo sequence	Spin echo single-shot EPI
TR	ms	4.2	465	9.1	1542
TE	ms	2.1	110	4.6	71
Flip angle	degree	18	90	50	90
Refocus angle	degree	N/A	120	N/A	N/A
TSE factor		N/A	78	N/A	N/A
FOV	mm	360 x 252	380 x 308	350 x 288	360
Matrix (frequency x phase)		240 x 133	375 x 297	224 x 184	304
b-value	s/mm ²				0, 500, and 1000
Slice thickness	mm	1.5	2	3	7
No. of slices		116	90	60	25
No. of excitations		1	1	1	1
Fat suppression technique		SPAIR	SPIR	Water selective excitation (1-2-1 binominal excitation pulse)	SPIR
Respiratory control		Breath-hold	Navigator-echo-based, real-time resp.-gating and resp.-triggering technique	Breath-hold	Navigator-echo-based, real-time resp.-gating and resp.-triggering technique
Scan time of whole slices	min:sec	00:20.7	05:02.0	00:18.6	01:54.0

DWI, diffusion-weighted imaging; EPI, echo-planar imaging; eTHRIVE, enhanced 3D T1 high-resolution isotropic volume excitation; FS-T2WI, fat-suppressed T2-weighted imaging; N/A, not available; SPAIR, spectral attenuation with inversion recovery; SPIR, spectral presaturation with inversion recovery; T1WI, T1-weighted imaging; T2FFE, T2-fast field echo; TSE, turbo spin echo; VISTA, volume isotropic turbo spin echo acquisition.

(1) lesions with a diameter ≤ 10 mm, and (2) lesions with a diameter > 10 mm. The AUCs of the four imaging data sets were nonparametrically compared using the ROCPLLOT macro (SAS Institute, Cary, NC, USA). First, a multiple comparison of AUCs was performed among four imaging data sets. If it showed a statistically significant difference, then pairwise comparisons of their AUCs were performed.

The kappa statistic was used to measure the inter-reader agreement for each pair of readers. The kappa value was calculated to assess the inter-reader agreement based on the following criteria: ≤ 0.20 , poor agreement; 0.20–0.40, fair agreement; 0.41–0.60, moderate agreement; 0.61–0.80, good agreement; and ≥ 0.81 , excellent agreement. All statistical analyses were performed with JMP software ver. 12.0 (SAS Institute). P values < 0.05 were considered significant for each analysis.

Results

The lesion-to-nonlesion contrast ratios between the hemangiomas and metastatic tumors

The lesion-to-nonlesion CRs of the 3D T1WI, 3D FS-T2WI, and T2FFE imaging in the HBP of the Gd-EOB-MRI demonstrated normal distributions: 3D T1WI, reader 1, $P = 0.52$, reader 2, $P = 0.97$; 3D FS-T2WI, reader 1, $P = 0.11$, reader 2, $P = 0.65$; and T2FFE imaging, reader 1, $P = 0.72$, reader 2, $P = 0.24$. The ICCs of the lesion-to-nonlesion CRs of the 3D T1WI, 3D FS-T2WI, and T2FFE imaging in the HBP of the Gd-EOB-MRI between the two readers were as follows: 3D T1WI, 0.99 (95% confidence interval [CI]: 0.98–0.99); 3D FS-T2WI, 0.98 (95% CI: 0.98–0.99); and T2FFE imaging, 0.98 (95% CI, 0.98–0.99), respectively. Excellent interobserver agreement was thus obtained.

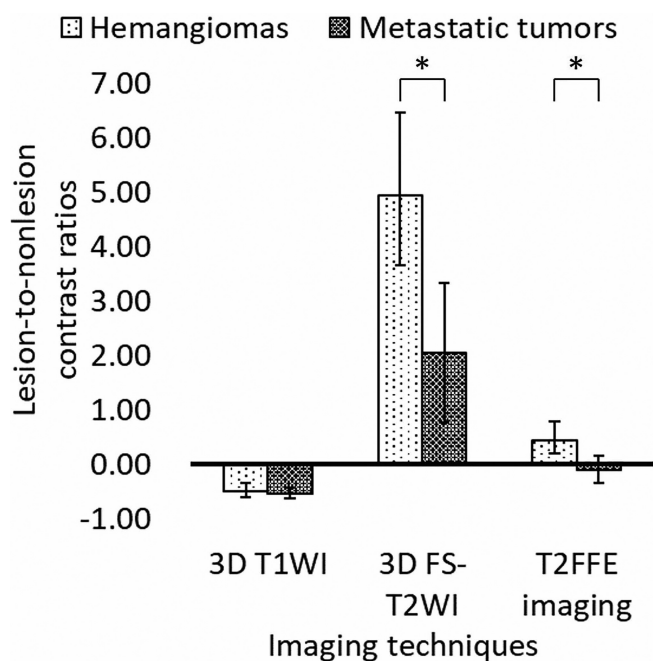


Fig. 2 The lesion-to-nonlesion CRs of 3D T1WI, 3D FS-T2WI, and T2FFE imaging in the hepatobiliary phase of Gd-EOB-MRI, which were averaged values using all data from the two readers. The mean \pm SD of the lesion-to-nonlesion CRs of 3D T1WI, 3D FS-T2WI, and T2FFE imaging in the hepatobiliary phase of Gd-EOB-MRI of the hemangiomas and the metastatic tumors were as follows: 3D T1WI, -0.51 ± 0.15 and -0.53 ± 0.11 ; 3D FS-T2WI, 4.94 ± 1.52 and 2.04 ± 1.29 ; T2FFE imaging, 0.44 ± 0.34 and -0.10 ± 0.25 . The 3D FS-T2WI and T2FFE imaging showed that the lesion-to-nonlesion CR of the hemangiomas was significantly higher than that of the metastatic tumors (*: $P < 0.05$). CR, contrast ratio; FS-T2WI, fat-suppressed T2-weighted imaging; Gd-EOB-MRI, gadoxetic acid-enhanced MRI; SD, standard deviation; T1WI, T1-weighted imaging; T2FFE, T2-fast field echo.

Figure 2 shows the lesion-to-nonlesion CRs of the 3D T1WI, 3D FS-T2WI, and T2FFE imaging in the HBP of the Gd-EOB-MRI, which were averaged values using all data from the two readers. The mean \pm standard deviations (SDs) of the averaged lesion-to-nonlesion CRs of the hemangiomas and the metastatic tumors were as follows: 3D T1WI, -0.51 ± 0.15 and -0.53 ± 0.11 ; 3D FS-T2WI, 4.94 ± 1.52 and 2.04 ± 1.29 ; and T2FFE imaging, 0.44 ± 0.34 and -0.10 ± 0.25 . The 3D FS-T2WI and T2FFE imaging showed that the lesion-to-nonlesion CR of the hemangiomas was significantly higher than that of the metastatic tumors ($P < 0.05$). The 3D FS-T2WI depicted all the hemangiomas and metastatic tumors as high-SI lesions, which means that the lesion-to-nonlesion CRs of the hemangiomas and metastatic tumors were > 0 .

In contrast, the T2FFE imaging could depict all hemangiomas as high-SI lesions (the lesion-to-nonlesion CRs were > 0), and it depicted most of the metastatic tumors as iso- or low-SI

lesions (the lesion-to-nonlesion CRs were ≤ 0). The 3D T1WI showed no significant difference in lesion-to-nonlesion CRs between the hemangiomas and metastatic tumors ($P = 0.52$, 95% CI: -0.03 - 0.06). Both types of lesions were depicted as low-SI.

Representative images of 3D T1WI, 3D FS-T2WI, and T2FFE imaging of the hemangiomas and the metastatic tumors are provided in Figs. 3–6.

The diagnostic accuracy for differentiating hemangiomas from metastatic tumors

For both readers, a multiple comparison of AUCs among four imaging data sets showed significant differences (P values of two readers were: for lesions ≤ 10 mm, < 0.0001 , and 0.0009 ; and for lesions > 10 mm, < 0.0001 , and 0.001). Pairwise comparisons of AUCs between pairs of imaging data sets calculated by the ROC analysis of the two readers are given in Table 3. For both readers, the AUCs of 3D FS-T2WI alone, the combination of 3D FS-T2WI and T2FFE imaging in the HBP of Gd-EOB-MRI, and the combination of 3D FS-T2WI and DWI with the b-value of 1000 s/mm^2 and ADC map were significantly higher than the AUC of dynamic Gd-EOB-MRI ($P < 0.05$). One reader showed that the AUC of the combination of 3D FS-T2WI and T2FFE imaging in the HBP of Gd-EOB-MRI was significantly higher than that of 3D FS-T2WI alone, but the other reader did not. However, both readers showed that there was no significant difference in the AUCs between 3D FS-T2WI and the combination of 3D FS-T2WI and DWI with the b-value of 1000 s/mm^2 and an ADC map, and between the combination of 3D FS-T2WI and T2FFE imaging in the HBP of Gd-EOB-MRI and the combination of 3D FS-T2WI and DWI with the b-value of 1000 s/mm^2 and an ADC map. Regardless of the lesions' sizes, the AUC results showed a similar trend among the four different imaging data sets.

The inter-reader agreement for each pair of readers

The results of the kappa statistic used to measure the inter-reader agreement for two readers are provided in Table 4. The results demonstrated that 3D FS-T2WI alone, the combination of 3D FS-T2WI and T2FFE imaging in the HBP of Gd-EOB-MRI, and the combination of 3D FS-T2WI and DWI with the b-value of 1000 s/mm^2 and an ADC map showed excellent inter-reader agreement regardless of the lesion size ($P < 0.05$). However, dynamic Gd-EOB-MRI showed poor agreement for the ≤ 10 -mm lesion group and fair agreement for the > 10 -mm group ($P < 0.05$).

Discussion

Our analyses revealed that in the HBP of Gd-EOB-MRI, the T2FFE imaging showed the hemangiomas as hyperintense and most of the metastatic tumors as iso- or hypointense, whereas the 3D T1WI showed both hemangiomas and metastatic tumors as hypointense, and the 3D FS-T2WI showed

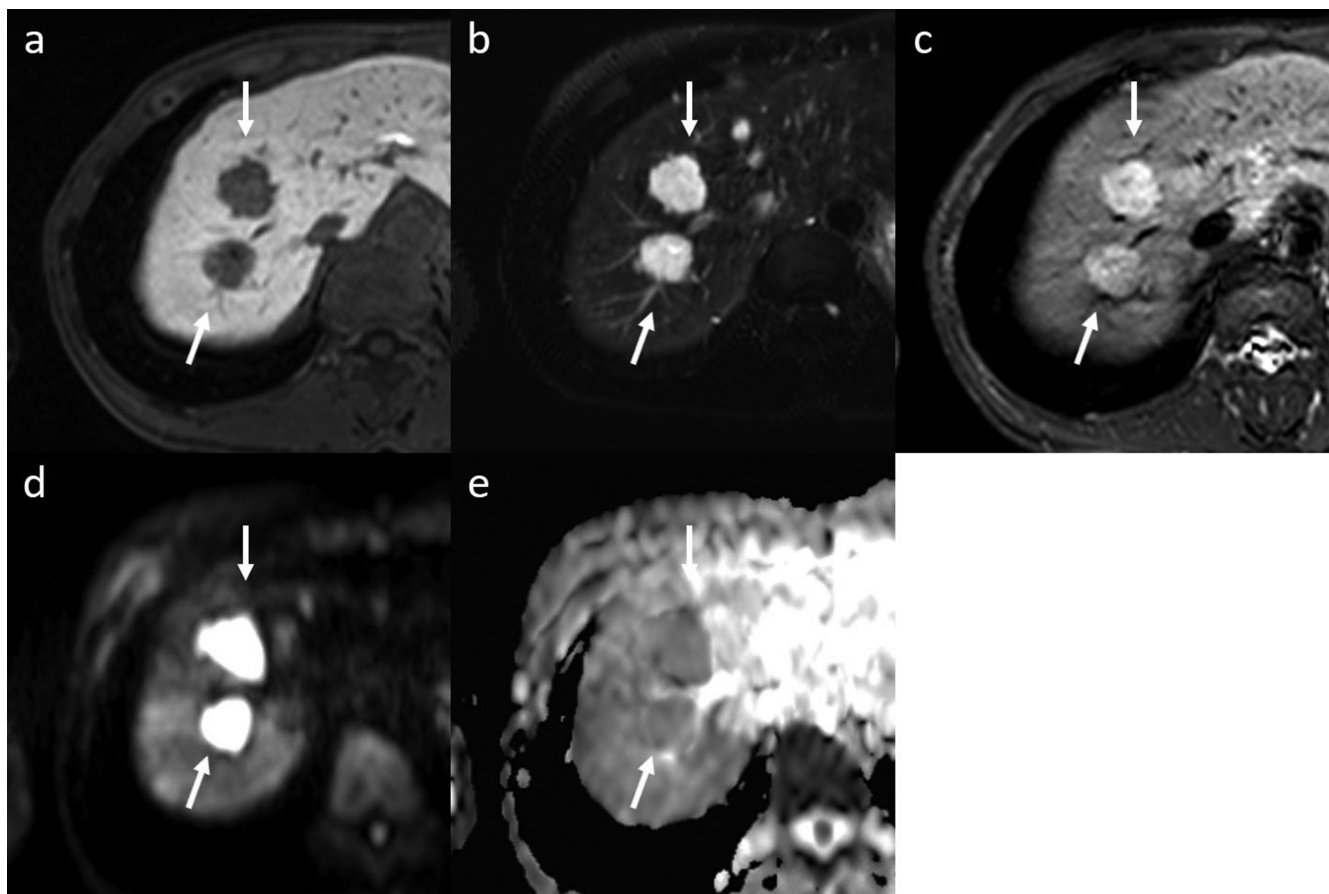


Fig. 3 A 56-yr-old female with hemangioma in segments 7 and 8 of the liver (arrows). (a) 3D T1WI in the HBP of the Gd-EOB-MRI, (b) 3D FS-T2WI, (c) T2FFE imaging in the HBP of the Gd-EOB-MRI, (d) DWI with the b-value of 1000 s/mm^2 , and (e) the ADC map. Two hemangiomas show hypointensity on 3D T1WI but hyperintensity on the 3D FS-T2WI, T2FFE imaging, and DWI. The lesion-to-nonlesion CRs of the hemangioma in segment 7 of the liver were as follows: 3D T1WI, -0.46 ; 3D FS-T2WI, 4.65 ; and T2FFE imaging, 0.67 . The averaged image interpretation scores of the two readers were as follows: (1) 3D FS-T2WI alone, 1.0 ; (2) the combination of 3D FS-T2WI and T2FFE imaging in the HBP of Gd-EOB-MRI, 1.0 ; (3) the combination of 3D FS-T2WI and DWI with the b-value of 1000 s/mm^2 and ADC, 2.5 ; and (4) dynamic Gd-EOB-MRI, 2.0 . The ADC of the hemangioma was $1.91 \times 10^{-3} \text{ mm}^2/\text{s}$. The lesion-to-nonlesion CRs of the hemangioma in segment 8 of the liver were as follows: 3D T1WI, -0.48 ; 3D FS-T2WI, 5.21 ; and T2FFE imaging, 0.45 . The averaged image interpretation scores of the two readers were as follows: (1) 3D FS-T2WI alone, 1.0 ; (2) the combination of 3D FS-T2WI and T2FFE imaging in HBP of Gd-EOB-MRI, 1.0 ; (3) the combination of 3D FS-T2WI, DWI with the b-value of 1000 s/mm^2 and ADC, 2.5 ; and (4) dynamic Gd-EOB-MRI, 2.5 . The ADC of the hemangioma was $1.62 \times 10^{-3} \text{ mm}^2/\text{s}$. ADC, apparent diffusion coefficient; CR, contrast ratio; DWI, diffusion-weighted imaging; FS-T2WI, fat-suppressed T2-weighted imaging; Gd-EOB-MRI, gadoteric acid-enhanced MRI; HBP, hepatobiliary phase; T1WI, T1-weighted imaging; T2FFE, T2-fast field echo.

both hemangiomas and metastatic tumors as hyperintense. The T2-enhanced spin-echo imaging with the time-reversed GRE sequence (which we call the T2FFE sequence) in the HBP of Gd-EOB-MRI could be helpful to differentiate hemangiomas from metastatic tumors. The T2FFE imaging may provide an easy interpreting method to differentiate liver hemangiomas and metastatic tumors with which we can judge whether a lesion's SI is hyper-, iso-, or hypointense.

The T2FFE sequence can clearly reflect slight differences in the SI between the liver parenchyma and liver lesions, namely, the T2 relaxation times or the ratio of T1 to T2 (T1/T2) relaxation times.³⁰ The T2FFE sequence without

contrast enhancement shows T2-weighted contrast.^{17,18} In contrast, T2FFE imaging in the HBP of Gd-EOB-MRI is thought to reflect both the T2 contrast and the T1 shortening effect of the uptake or pooling of gadoteric acid in the liver parenchyma and liver lesions.^{17,18} We observed no significant differences in the lesion-to-nonlesion CRs of 3D T1WI in the HBP of Gd-EOB-MRI, as described in another study¹⁸; therefore, the T1 shortening effect of gadoteric acid might not have a significant influence on the difference between the signal intensities of hemangiomas and metastatic tumors on T2FFE imaging.

There are two possible factors explaining why the T2FFE imaging depicted the hemangiomas as hyperintense and most

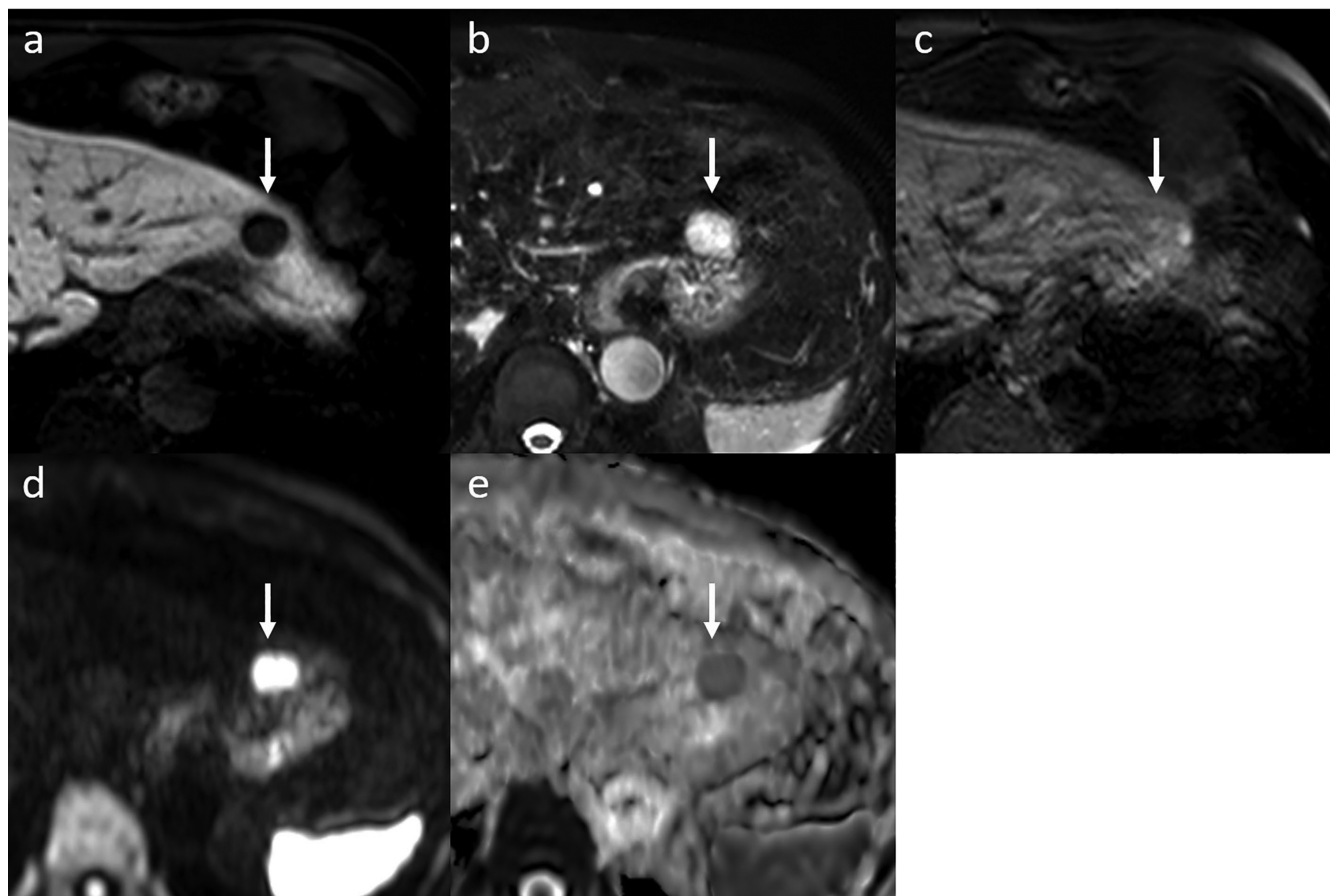


Fig. 4 A 63-yr-old male with a metastatic tumor in segment 2 of the liver (arrows). The primary metastatic tumor was a malignant gastrointestinal stromal tumor of the stomach. (a) 3D T1WI in the HBP of the Gd-EOB-MRI, (b) 3D FS-T2WI, (c) T2FFE imaging in the HBP of the Gd-EOB-MRI, (d) DWI with the b-value of 1000 s/mm^2 , and (e) the ADC map. The metastatic tumor showed hypointensity on the 3D T1WI and iso-intensity on the T2FFE imaging but hyperintensity on the 3D FS-T2WI and DWI. The lesion-to-nonlesion CRs of the metastatic tumor in segment 2 of the liver were as follows: 3D T1WI, -0.71 ; 3D FS-T2WI, 0.38 , and T2FFE imaging, 0.05 . The averaged image interpretation scores of the two readers were as follows: (1) 3D FS-T2WI alone, 2.5 ; (2) the combination of 3D FS-T2WI and T2FFE imaging in the HBP of Gd-EOB-MRI, 3.5 ; (3) the combination of 3D FS-T2WI and DWI with the b-value of 1000 s/mm^2 and an ADC, 2.5 ; and (4) dynamic Gd-EOB-MRI, 3.5 . The ADC of the metastatic tumor was $1.53 \times 10^{-3} \text{ mm}^2/\text{s}$. ADC, apparent diffusion coefficient; CR, contrast ratio; DWI, diffusion-weighted imaging; FS-T2WI, fat-suppressed T2-weighted imaging; Gd-EOB-MRI, gadoteric acid-enhanced MRI; HBP, hepatobiliary phase; T1WI, T1-weighted imaging; T2FFE, T2-fast field echo.

of the metastatic tumors as iso- or hypointense. One possible factor is the differences in the T2 contrast of liver lesions, which played an important role in the determination of the lesion-to-nonlesion CRs of the T2FFE imaging. The hemangiomas showed significantly higher SIs compared to the metastatic tumors. Another possible factor is the change of the liver parenchymal SI that was greatly influenced by the T1 shortening effect of gadoteric acid compared to liver lesions in the HBP of the Gd-EOB-MRI because of the uptake of gadoteric acid from hepatocytes.¹⁸

We suspect that increased liver parenchymal SI on T2FFE imaging in the HBP could unexpectedly become a reference point of the signal level for the interpretation of the SIs of hemangiomas or metastatic tumors compared with liver parenchymal SIs.^{17,18} Thus, we speculated that this is why the 3D FS-T2WI depicted all of the

hemangiomas and metastatic tumors as hyperintense, but the T2FFE imaging in the HBP of Gd-EOB-MRI could depict all hemangiomas as hyperintense and most of the metastatic tumors as iso- or hypointense.

Several imaging techniques have been applied to the differentiation of hemangiomas and metastatic tumors, including DWI, ADC, diffusion tensor imaging, and T1 and T2 relaxation times.^{28,30–32} In clinical practice, if the arterial-phase images of Gd-EOB-MRI are hampered by artifacts, radiologists may interpret other MRI findings (especially those obtained with FS-T2WI, DWI, and an ADC map) to diagnose liver lesions on Gd-EOB-MRI. Regarding the diagnostic accuracy for differentiating hemangiomas from metastatic tumors, in the present study, the AUCs of the combination of 3D FS-T2WI and T2FFE imaging in the HBP of Gd-EOB-MRI and the combination of 3D FS-T2WI and DWI with the

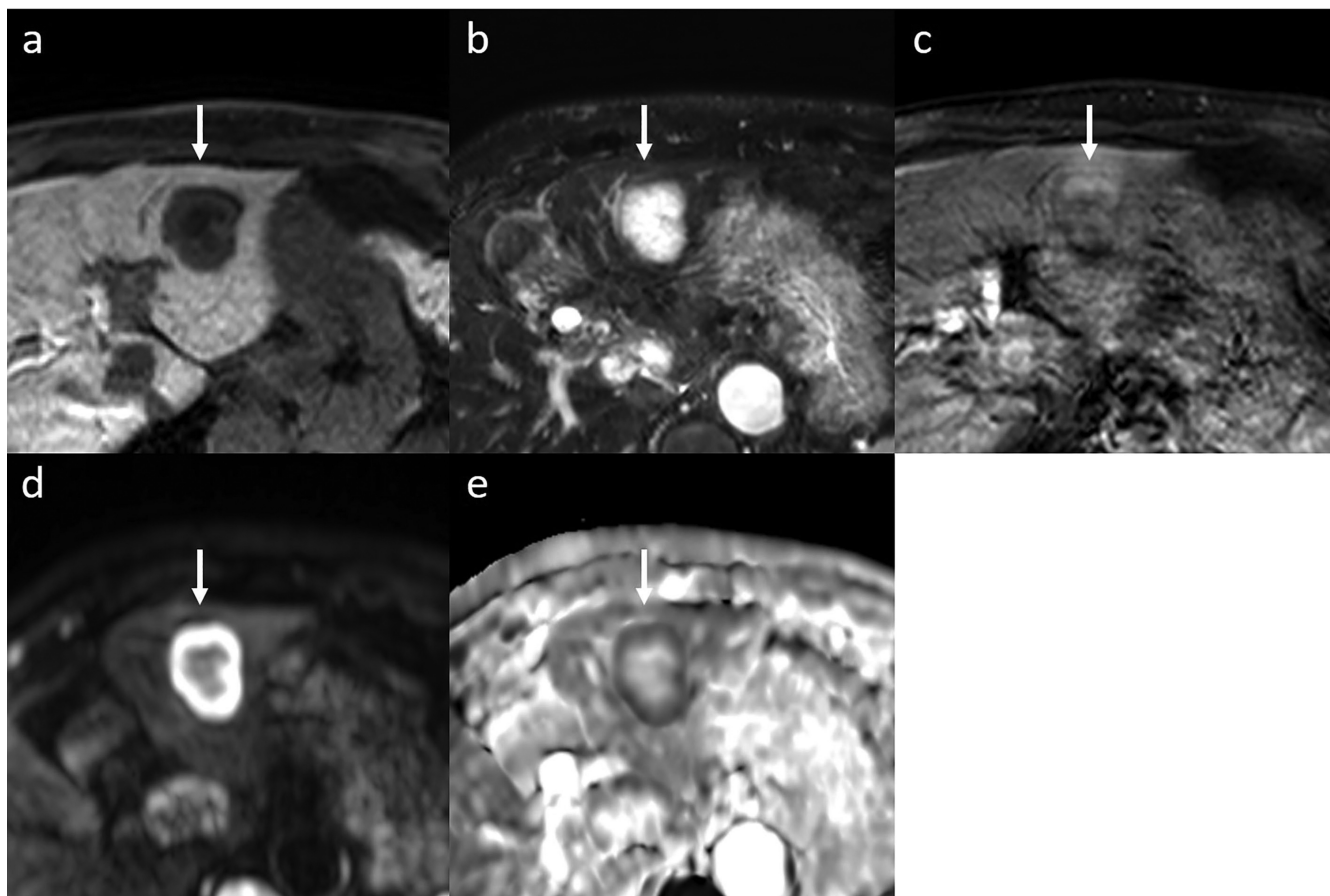


Fig. 5 An 83-yr-old male with a metastatic tumor in segment 3 of the liver (arrows). The primary metastatic tumor was a mucinous adenocarcinoma of the sigmoid colon. This case was difficult to be distinguished from hemangioma because of the lesion's high signal intensity on the T2FFE sequence. (a) 3D T1WI in the HBP of the Gd-EOB-MRI, (b) 3D FS-T2WI, (c) T2FFE imaging in the HBP of the Gd-EOB-MRI, (d) DWI with the b-value of 1000 s/mm², and (e) the ADC map. The metastatic tumor showed hypointensity on 3D T1WI and hyperintensity on 3D FS-T2WI and DWI. The T2FFE imaging depicted inhomogeneous SI, but it showed iso- or low SI in > 50% of the lesion's area on T2FFE imaging. The lesion-to-nonlesion CRs of the metastatic tumor in segment 3 of the liver were as follows: 3D T1WI, -0.67; 3D FS-T2WI, 0.35; and T2FFE imaging, 0.24. The averaged image interpretation scores of the two readers were as follows: (1) 3D FS-T2WI alone, 2.5; (2) the combination of 3D FS-T2WI and T2FFE imaging in the HBP of Gd-EOB-MRI, 3.5; (3) the combination of 3D FS-T2WI and DWI with the b-value of 1000 s/mm² and an ADC, 4.0; and (4) dynamic Gd-EOB-MRI, 3.5. The ADC of the metastatic tumor was 1.50×10^{-3} mm²/s. ADC, apparent diffusion coefficient; CR, contrast ratio; DWI, diffusion-weighted imaging; FS-T2WI, fat-suppressed T2-weighted imaging; Gd-EOB-MRI, gadoteric acid-enhanced MRI; HBP, hepatobiliary phase; SI, signal intensity; T1WI, T1-weighted imaging; T2FFE, T2-fast field echo.

b-value of 1000 s/mm² and an ADC map were significantly higher than that of dynamic Gd-EOB-MRI. The reasons why the dynamic Gd-EOB-MRI showed lower diagnostic accuracy are unknown, but we speculated that a few factors such as poor-quality arterial-phase images of Gd-EOB-MRI (seen in 9/61 patients [14.8%] in this study)³³ and poor visualization of dot-like or ring enhancement might have influenced the results.

One of our two readers obtained a significantly better diagnostic performance of the combination of 3D FS-T2WI and T2FFE imaging compared to that of the 3D FS-T2WI alone. This result indicated that the additional scan of T2FFE imaging in the HBP of Gd-EOB-MRI provided helpful information for one reader to differentiate hemangiomas from metastatic tumors. However, for the other reader, there was no significant

increase in the diagnostic performance by adding T2FFE imaging compared to 3D FS-T2WI alone. The addition of T2FFE imaging might not be necessary for radiologists who are well experienced in interpreting liver lesions on FS-T2WI.

We also observed that the combination of 3D FS-T2WI and T2FFE imaging in the HBP of Gd-EOB-MRI and the combination of 3D FS-T2WI and DWI with the b-value of 1000 s/mm² and an ADC map had equivalent diagnostic accuracy for differentiating hemangiomas from metastatic tumors. This result indicated that the combination of 3D FS-T2WI and T2FFE imaging in the HBP of Gd-EOB-MRI might be helpful in the diagnosis of hemangiomas and/or metastatic tumors on liver MRI, as were the combination of 3D-FD-T2WI, DWI, and ADC. Although it was not a statistically significant difference, the AUCs of the combination

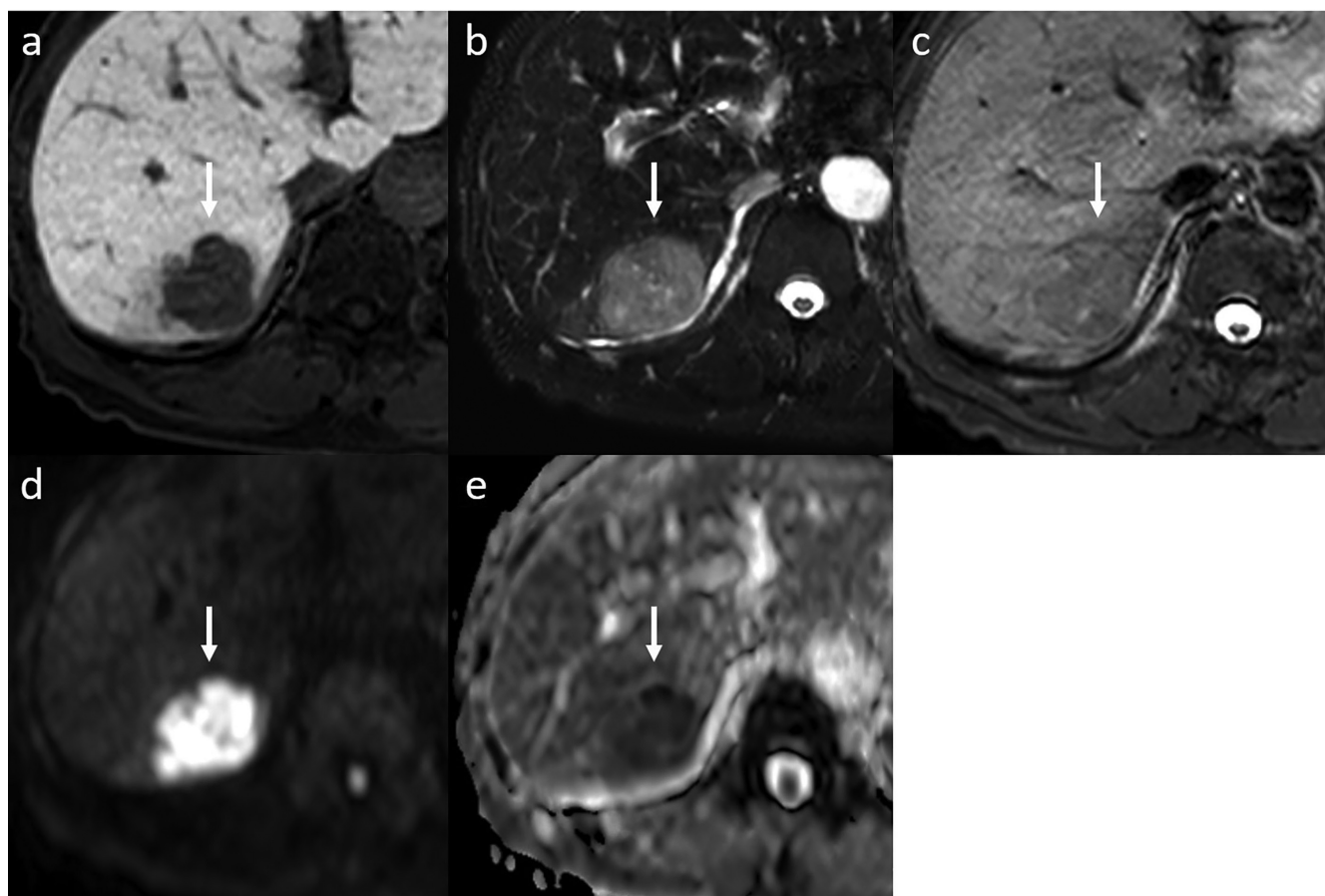


Fig. 6 A 75-yr-old male with a metastatic tumor in segment 7 of the liver (arrows). The primary metastatic tumor was an adenocarcinoma of the rectum. (a) 3D T1WI in the HBP of the Gd-EOB-MRI, (b) 3D FS-T2WI, (c) T2FFE imaging in the HBP of the Gd-EOB-MRI, (d) DWI with the b-value of 1000 s/mm², and (e) the ADC map. The metastatic tumor showed hypointensity on the 3D T1WI and the T2FFE imaging but slight hyperintensity on the 3D FS-T2WI and hyperintensity on DWI. The lesion-to-nonlesion CRs of the metastatic tumor in segment 6 of the liver were as follows: 3D T1WI, -0.66; 3D FS-T2WI, 2.78; and T2FFE imaging, -0.22. The averaged image interpretation scores of the two readers were as follows: (1) 3D FS-T2WI alone, 4.0; (2) the combination of 3D FS-T2WI and T2FFE imaging in the HBP of Gd-EOB-MRI, 4.0; (3) the combination of 3D FS-T2WI and DWI with the b-value of 1000 s/mm² and an ADC, 4.0; and (4) dynamic Gd-EOB-MRI, 3.5. The ADC of the metastatic tumor was 0.85×10^{-3} mm²/s. ADC, apparent diffusion coefficient; CR, contrast ratio; DWI, diffusion-weighted imaging; FS-T2WI, fat-suppressed T2-weighted imaging; Gd-EOB-MRI, gadoteric acid-enhanced MRI; HBP, hepatobiliary phase; T1WI, T1-weighted imaging; T2FFE, T2-fast field echo.

of 3D FS-T2WI and T2FFE imaging were higher than those of the combination of 3D FS-T2WI, DWI, and ADC. The combination of 3D FS-T2WI and T2FFE imaging in the HBP of Gd-EOB-MRI may give other useful information to radiologists when they diagnose liver hemangioma and metastatic tumor using 3D FS-T2WI, DWI, and ADC. The T2FFE sequence is a commercially available imaging technique and does not need any special applications or software. The scan time of T2FFE imaging of the whole liver in this study was only 18.4 sec, and thus the images can be acquired during breath-holding and the sequence is not time-consuming.

This study has several limitations. First, the T2FFE sequence with high FAs (e.g., a FA of 50° at 1.5T) cannot be applied to a 3.0T scanner due to the limitation of SAR.¹⁸ While it is known that the T1 relaxation time at 3.0T is longer than that at 1.5T, in our experience, the SAR limits the FA to

around 30°, and the T2FFE sequence with a FA of 30° at 3.0T does not provide as good contrast as at 1.5T. Thus, the T2FFE sequence cannot be used for a 3.0T scanner. Second, when each reader evaluated the lesion signal intensities for a case with multiple liver lesions, the reader might conclude that all of the lesions had the same etiology. A bias could thus be present. Third, it is clinically important to investigate whether the T2FFE sequence is useful in the differentiation of lesions showing atypical findings. However, there was no diagnostic standard to classify such a lesion into hemangiomas or metastatic tumors in this study. In addition, if any metastatic tumors had a large necrotic area, we might have accidentally excluded them from the present analyses by assuming that they were liver cysts. In this study, we did not consider how necrotic areas affect the interpretation of the lesion's SI on the T2FFE sequence. Fourth, the

Table 3 The AUCs and the two readers' interpretations to differentiate hemangiomas from metastatic tumors

	AUCs (95% CI)				P values					
	(1) 3D FS-T2WI alone	(2) 3D FS-T2WI and T2FFE imaging	(3) 3D FS-T2WI, DWI, and ADC map	(4) Dynamic Gd-EOB-MRI	(1) vs. (2)	(1) vs. (3)	(1) vs. (4)	(2) vs. (3)	(2) vs. (4)	(3) vs. (4)
≤ 10 mm:										
Reader 1	0.85 (0.72–0.92)	0.94 (0.83–1.00)	0.90 (0.78–1.00)	0.62 (0.44–0.81)	0.0064*	0.09	0.015*	0.31	0.0002*	<0.0001*
Reader 2	0.91 (0.80–0.97)	0.94 (0.83–1.00)	0.87 (0.73–1.00)	0.67 (0.48–0.86)	0.15	0.84	0.021*	0.29	0.017*	0.003*
> 10 mm:										
Reader 1	0.88 (0.81–0.92)	0.96 (0.91–1.00)	0.89 (0.80–0.98)	0.76 (0.66–0.86)	0.012*	0.21	0.021*	0.31	0.0004*	<0.0001*
Reader 2	0.97 (0.91–0.99)	0.95 (0.90–1.00)	0.95 (0.89–1.00)	0.71 (0.59–0.84)	0.55	0.99	0.0001*	0.6	<0.0001*	0.0003*

* $P < 0.05$. ADC, apparent diffusion coefficient; AUC, area under the curve; CI, confidence interval; DWI, diffusion-weighted imaging; FS-T2WI, fat-suppressed T2-weighted imaging; Gd-EOB-MRI, gadoxetic acid-enhanced MRI; T2FFE imaging, T2-enhanced spin-echo imaging using the time-reversed gradient echo sequence.

Table 4 Kappa values (95% CI) of the inter-reader agreement of the two readers for each combination of imaging data set

	(1) 3D FS-T2WI alone	(2) 3D FS-T2WI and T2FFE imaging	(3) 3D FS-T2WI, DWI, and ADC map	(4) Dynamic Gd-EOB-MRI
≤ 10 mm	0.83 (0.67–0.98)	1.00 (1.00–1.00)	0.91 (0.79–1.00)	0.28 (0.04–0.52)
> 10 mm	0.79 (0.67–0.90)	0.93 (0.85–1.00)	0.87 (0.77–0.96)	0.49 (0.36–0.63)

ADC, apparent diffusion coefficient; CI, confidence interval; DWI, diffusion-weighted imaging; FS-T2WI, fat-suppressed T2-weighted imaging; Gd-EOB-MRI, gadoxetic acid-enhanced MRI; T2FFE imaging, T2-enhanced spin-echo imaging using the time-reversed gradient echo sequence.

Appendix 1. The initial diagnosis and actual outcome of liver lesions in the 56 patients who were excluded by criteria.

Number of patients	Initial diagnosis on Gd-EOB-MRI	Outcome on follow-up studies
7	Hemangioma	No follow-up study nor pathology result
12	Metastatic tumor	No follow-up study nor pathology result
4	Hemangioma or metastatic tumor	No change in the lesion on follow-up studies, difficulty in diagnosis because of small lesions and no pathology result.
1	Metastatic tumor or simple cyst	No change in the lesion on follow-up studies, difficulty in diagnosis because of small lesions and no pathology result.
1	Hemangioma or epithelioid hemangioendothelioma	No change in the lesion on follow-up studies, difficulty in diagnosis and no pathology result.
2	Focal nodular hyperplasia	No follow-up study nor pathology result
1	Sarcoidosis	No follow-up study nor pathology result
4	Abscess and infected cyst	No follow-up study nor pathology result
9	Nonspecific findings that were difficult to diagnosis	No change in the lesion on follow-up studies, difficulty in diagnosis and no pathology result.
15	Hypovascular nodule in patients with chronic liver disease	No change in the lesion on follow-up studies, difficulty in diagnosis and no pathology result.

Gd-EOB-MRI, gadoxetic acid-enhanced MRI.

diagnostic performance of T2FFE imaging alone was not evaluated because some lesions showed obscure contours on this sequence. Therefore, the efficacy of a combination of 3D FS-T2WI and T2FFE imaging was compared with that of 3D FS-T2WI alone. We did not evaluate the additional value of the T2FFE imaging to DWI alone or dynamic Gd-EOB-MRI. The comparison of DWI alone versus the combination of T2FFE imaging and DWI or the comparison of dynamic Gd-EOB-MRI alone versus the combination of T2FFE imaging and dynamic Gd-EOB-MRI may also prove the usefulness of T2FFE imaging for differentiation between hemangiomas and metastatic tumors. We judged that it might be clinically meaningful to compare data set (3) with data set (4). These data sets are used for differentiation between hemangiomas and metastatic tumors in daily practice.

Conclusion

The combination of 3D FS-T2WI and T2FFE imaging in the HBP of Gd-EOB-MRI achieved an accuracy equal to that of the combination of 3D FS-T2WI, DWI, and ADC. A simple interpretation of lesion SI using this combination modality was helpful to differentiate liver hemangiomas from metastatic tumors.

Acknowledgments

This work was supported by JSPS KAKENHI Grant Number JP20K08028.

Conflicts of Interest

Masami Yoneyama is an employee of Philips Electronics Japan. Other authors have no conflict of interest.

References

- Vogl TJ, Kümmel S, Hammerstingl R, et al. Liver tumors: comparison of MR imaging with Gd-EOB-DTPA and Gd-DTPA. *Radiology* 1996; 200:59–67.
- Seale MK, Catalano OA, Saini S, et al. Hepatobiliary-specific MR contrast agents: role in imaging the liver and biliary tree. *Radiographics* 2009; 29:1725–1748.
- Asayama Y, Tajima T, Nishie A, et al. Uptake of Gd-EOB-DTPA by hepatocellular carcinoma: radiologic-pathologic correlation with special reference to bile production. *Eur J Radiol* 2011; 80:e243–248.
- Takayama Y, Nishie A, Nakayama T, et al. Hypovascular hepatic nodule showing hypointensity in the hepatobiliary phase of gadoxetic acid-enhanced MRI in patients with chronic liver disease: prediction of malignant transformation. *Eur J Radiol* 2012; 81:3072–3078.
- Sirlin CB, Hussain HK, Jonas E, et al. Consensus report from the 6th International forum for liver MRI using gadoxetic acid. *J Magn Reson Imaging* 2014; 40:516–529.
- Fujita N, Nishie A, Asayama Y, et al. Significance of the signal intensity of gadoxetic acid-enhanced MR imaging for predicting the efficacy of hepatic arterial infusion chemotherapy in hepatocellular carcinoma. *Magn Reson Med Sci* 2016; 15:111–120.
- Goshima S, Kanematsu M, Watanabe H, et al. Hepatic hemangioma and metastasis: differentiation with gadoxetate disodium-enhanced 3-T MRI. *AJR Am J Roentgenol* 2010; 195:941–946.
- Ringe KI, Husarik DB, Sirlin CB, et al. Gadoxetate disodium-enhanced MRI of the liver: part 1, protocol optimization and lesion appearance in the noncirrhotic liver. *AJR Am J Roentgenol* 2010; 195:13–28.
- Motosugi U, Ichikawa T, Onohara K, et al. Distinguishing hepatic metastasis from hemangioma using gadoxetic acid-enhanced magnetic resonance imaging. *Invest Radiol* 2011; 46:359–365.
- Sofue K, Tsurusaki M, Tokue H, et al. Gd-EOB-DTPA-enhanced 3.0 T MR imaging: quantitative and qualitative comparison of hepatocyte-phase images obtained 10 min and 20 min after injection for the detection of liver metastases from colorectal carcinoma. *Eur Radiol* 2011; 21:2336–2343.
- Tamada T, Ito K, Yamamoto A, et al. Hepatic hemangiomas: evaluation of enhancement patterns at dynamic MRI with gadoxetate disodium. *AJR Am J Roentgenol* 2011; 196:824–830.
- Jeong HT, Kim MJ, Park MS, et al. Detection of liver metastases using gadoxetic-enhanced dynamic and 10- and 20-minute delayed phase MR imaging. *J Magn Reson Imaging* 2012; 35:635–643.
- Motosugi U, Ichikawa T, Araki T. Rules, roles, and room for discussion in gadoxetic acid-enhanced magnetic resonance liver imaging: current knowledge and future challenges. *Magn Reson Med Sci* 2013; 12:161–175.
- Haradome H, Grazioli L, Morone M, et al. T2-weighted and diffusion-weighted MRI for discriminating benign from malignant focal liver lesions: diagnostic abilities of single versus combined interpretations. *J Magn Reson Imaging* 2012; 35:1388–1396.
- Davenport MS, Bashir MR, Pietryga JA, et al. Dose-toxicity relationship of gadoxetate disodium and transient severe respiratory motion artifact. *AJR Am J Roentgenol* 2014; 203:796–802.
- Chavhan GB, Babyn PS, Jankharia BG, et al. Steady-state MR imaging sequences: physics, classification, and clinical applications. *Radiographics* 2008; 28:1147–1160.
- Yoneyama M, Nakamura M, Tabuchi T, et al. Reevaluation of T2-weighted fast field echo (T2FFE): application to rapid volumetric black-blood imaging. *Radiol Phys Technol* 2013; 6:305–312.
- Yoneyama M, Takayama Y, Nishie A, et al. Differentiation of hypointense nodules on gadoxetic acid-enhanced hepatobiliary-phase MRI using T2 enhanced spin-echo imaging with the time-reversed gradient echo sequence: an initial experience. *Eur J Radiol* 2017; 95:325–331.
- Jang HJ, Choi BI, Kim TK, et al. Atypical small hemangiomas of the liver: “bright dot” sign at two-phase spiral CT. *Radiology* 1998; 208:543–548.

20. Kim T, Federle MP, Baron RL, et al. Discrimination of small hepatic hemangiomas from hypervascular malignant tumors smaller than 3 cm with three-phase helical CT. *Radiology* 2001; 219:699–706.
21. Jang HJ, Kim TK, Lim HK, et al. Hepatic hemangioma: atypical appearances on CT, MR imaging, and sonography. *AJR Am J Roentgenol* 2003; 180:135–141.
22. Caseiro-Alves F, Brito J, Araujo AE, et al. Liver haemangioma: common and uncommon findings and how to improve the differential diagnosis. *Eur Radiol* 2007; 17:1544–1554.
23. Danet IM, Semelka RC, Leonardou P, et al. Spectrum of MRI appearances of untreated metastases of the liver. *AJR Am J Roentgenol* 2003; 181:809–817.
24. Takayama Y, Nishie A, Asayama Y, et al. Three-dimensional T2-weighted imaging for liver MRI: clinical values of tissue-specific variable refocusing flip-angle turbo spin echo imaging. *J Magn Reson Imaging* 2015; 41:339–346.
25. Shinozaki K, Yoshimitsu K, Irie H, et al. Comparison of test-injection method and fixed-time method for depiction of hepatocellular carcinoma using dynamic steady-state free precession magnetic resonance imaging. *J Comput Assist Tomogr* 2004; 28:628–634.
26. Soyer P, Dufresne AC, Somville E, et al. Hepatic cavernous hemangioma: appearance on T2-weighted fast spin-echo MR imaging with and without fat suppression. *AJR Am J Roentgenol* 1997; 168:461–465.
27. Hardie AD, Egbert RE, Rissing MS. Improved differentiation between hepatic hemangioma and metastases on diffusion-weighted MRI by measurement of standard deviation of apparent diffusion coefficient. *Clin Imaging* 2015; 39:654–658.
28. Namimoto T, Nakagawa M, Kizaki Y, et al. Characterization of liver tumors by diffusion-weighted imaging: comparison of diagnostic performance using the mean and minimum apparent diffusion coefficient. *J Comput Assist Tomogr* 2015; 39:453–461.
29. Granata V, Catalano O, Fusco R, et al. The target sign in colorectal liver metastases: an atypical Gd-EOB-DTPA “uptake” on the hepatobiliary phase of MR imaging. *Abdom Imaging* 2015; 40:2364–2371.
30. Farraher SW, Jara H, Chang KJ, et al. Differentiation of hepatocellular carcinoma and hepatic metastasis from cysts and hemangiomas with calculated T2 relaxation times and the T1/T2 relaxation times ratio. *J Magn Reson Imaging* 2006; 24:1333–1341.
31. Erturk SM, Ichikawa T, Kaya E, et al. Diffusion tensor imaging of cysts, hemangiomas, and metastases of the liver. *Acta Radiol* 2014; 55:654–660.
32. Saito K, Yoshimura N, Shirota N, et al. Distinguishing liver haemangiomas from metastatic tumours using gadolinium ethoxybenzyl diethylenetriamine pentaacetic acid-enhanced diffusion-weighted imaging at 1.5T MRI. *J Med Imaging Radiat Oncol* 2016; 60:599–606.
33. Motosugi U, Bannas P, Bookwalter CA, et al. An investigation of transient severe motion related to gadoxetic acid-enhanced MR imaging. *Radiology* 2016; 279:93–102.